Matching Pursuit based Removal of Cardiac Pulse-Related Artifacts in EEG/fMRI

Rainer Schneider, Stephan Lau, Levin Kuhlmann, Simon Vogrin, Maciej Gratkowski, Mark Cook,
Jens Haueisen

Abstract—Cardiac pulse-related artifacts in the EEG recorded simultaneously with fMRI are complex and highly variable. Their effective removal is an unsolved problem. Our aim is to develop an adaptive removal algorithm based on the matching pursuit (MP) technique and to compare it to established methods using a visual evoked potential (VEP). We recorded the VEP inside the static magnetic field of an MR scanner (with artifacts) as well as in an electrically shielded room (artifact free). The MP-based artifact removal outperformed average artifact subtraction (AAS) and optimal basis set removal (OBS) in terms of restoring the EEG field map topography of the VEP. Subsequently, a dipole model was fitted to the VEP under each condition using a realistic boundary element head model. The source location of the VEP recorded inside the MR scanner was closest to that of the artifact free VEP after cleaning with the MP-based algorithm as well as with AAS. While none of the tested algorithms offered complete removal, MP showed promising results due to its ability to adapt to variations of latency, frequency and amplitude of individual artifact occurrences while still utilizing a common template.

Keywords—matching pursuit, ballistocardiogram, artifact removal, EEG/fMRI.

I. INTRODUCTION

MULTIMODAL non-invasive measurements of brain function open new windows for basic research and clinical routine. Single modalities like EEG, MEG, fMRI and PET provide only an incomplete picture of the underlying brain activity since their sensitivity is limited and they often provide qualitatively and quantitatively different information. For instance, EEG captures electrical brain activity directly and has a high temporal resolution but the spatial resolution in source localization procedures is strongly limited by the signal-to-noise ratio. Measurement techniques like fMRI only indirectly address electrical brain function through the correlation of metabolic and electric function. fMRI provides a relatively high spatial resolution, but a poor temporal resolution. A combination of the complementary techniques of EEG and fMRI thus considerably broadens our view on brain function and dysfunction. Ideally, simultaneous EEG/fMRI measurements are carried out. However, besides technical problems, two major types of artifacts compromise the EEG recorded during fMRI acquisition: the gradient artifact and cardiac pulse-related artifacts. Here, we consider the latter.

Cardiac pulse related artifacts are complex "mesogeneous" artifacts as they follow from an interaction between the cardiovascular system (endogenous) and static B_0 field (exogenous). They include the ballistocardiogram (BCG) from local pulsatile movements of scalp vessels adjacent to electrodes, and effects from abrupt changes in blood velocity leading to voltage difference on opposite sides of a moving conductor through which an electric current is flowing in a static magnetic field – the Hall effect [1]. The amplitude of cardiac pulse related artifacts is about 10-100 times larger than the EEG. Additionally, these artifacts are non-stationary including variations in morphology and amplitude both over time and channels. Moreover, different realizations in different recording setups (MRI scanner, EEG system) and individuals are observed. Consequently, the automated removal of cardiac pulse related artifacts requires adaptive algorithms.

The aim of our work is the development of such an adaptive algorithm. As the basis for this algorithm we choose the matching pursuit decomposition method because it is able to adaptively decompose signals into parameterized atoms. Based on the parameters of the atoms used for the decomposition one can perform separation of artifacts and components of interest. We compare the performance of our method against two established methods: Average Artifact Subtraction (AAS) [2] and Optimal Basis Sets (OBS) [3].

R. Schneider is with the Institute of Biomedical Engineering and Informatics, Technical University Ilmenau, Ilmenau, D- 98693, Germany (e-mail: rainer.schneider@tu-ilmenau.de).

S. Lau is with the Institute of Biomedical Engineering and Informatics, Technical University Ilmenau, Ilmenau, D- 98693, Germany, as well as the NeuroEngineering Laboratory, Department of Electrical and Electronic Engineering, The University of Melbourne, Melbourne, Australia (e-mail: stephan.lau@tu-ilmenau.de).

L. Kuhlmann is with the Department of Optometry and Vision Sciences and the Department of Electrical and Electronic Engineering, The University of Melbourne, Melbourne 3010, Australia (e-mail: levink@unimelb.edu.au).

S. Vogrin is with the Centre for Clinical Neurosciences, St. Vincent's Hospital Melbourne, Fitzroy 3065, Australia (e-mail: simon.vogrin@svhm.org.au).

M. Gratkowski is with the Institute of Biomedical Engineering and Informatics, Technical University Ilmenau, Ilmenau, D- 98693, Germany (e-mail: maciej.gratkowski@tu-ilmenau.de).

M. Cook is with the Centre for Clinical Neurosciences, St. Vincent's Hospital Melbourne, Fitzroy 3065, Australia (e-mail: mark.cook@svhm.org.au).

J. Haueisen is with the Institute of Biomedical Engineering and Informatics, Technical University Ilmenau, Ilmenau, D- 98693, Germany (e-mail: jens.haueisen@tu-ilmenau.de).

II. METHODS

A. Recording Setup and Acquisition

Two EEG datasets were recorded from a healthy participant after obtaining informed consent (HREC-A 034/08,

World Academy of Science, Engineering and Technology
International Journal of Biomedical and Biological Engineering
Vol:5, No:8, 2011

St Vincent's Hospital Melbourne). The two acquisitions were performed using the same high density 128 channel MR-compatible electrode cap configuration (Maglink Quik-Cap, Neuroscan, Charlotte NC, USA) connected to an MR-compatible EEG acquisition system (Maglink RT, Neuroscan, Charlotte NC, USA) without any reapplication of cap electrodes. Both datasets involved recording visually evoked potentials from left hemifield stimulations, the first in an electrically shielded room with no static magnetic field and the second one inside the MR scanner (1.5T Magnetom Avanto, Siemens, Erlangen, Germany). No MR scanning sequences were run during this EEG acquisition to ensure measures allowed for controlling of pulse-related artifacts only, i.e. not concomitant with effects from independent EEG processing techniques required to correct for MR gradient artifacts.

In addition to the 128 sintered Ag/AgCl monopolar electrodes uniformly covering the scalp, two further sintered Ag/AgCl electrode pairs above and below the left eye and at the outer canthi of each eye were used to record the vertical and horizontal electrooculogram (EOG). The electrocardiogram (ECG) was recorded between an electrode 2 cm left of the sternum and one 2 cm inferiorly from the sternoclavicular joint. An MR-compatible pulse oximeter (Nonin 8600FO, Nonin Medical, Plymouth MN, USA) was connected via an isolated high level input channel.

EEG data were digitized using 24-bit ADC per channel, and stored in 32-bit data format. Amplifier sampling rates were 20 kHz in the electrically shielded room and 10 kHz inside the MR scanner, with respective analogue filters of DC-3.5 kHz and DC-2 kHz at -6 dB/Oct roll off.

B. Visual Stimulation Paradigm

The left hemifield was stimulated with a reversing black & white checkerboard pattern in the left half of the screen and a red circle in the center for the subject to focus on throughout the recording using the Stim2 presentation software (Neuroscan, Charlotte NC, USA). A 5 x 10 square checkerboard pattern reversal occurring at an interval of 240 ms (1280x1024 screen resolution @ 75 Hz refresh rate) provided 100 stimuli in an "active" phase of 24 seconds (followed by a 24 second "rest" phase section) for 7 cycles (or a total of 700 stimuli). Triggers for each stimulus presented were passed directly to the Maglink RT system and stored in the EEG data file for epoch processing. The continuous EEG during stimuli was acquired over approximately six minutes.

In the electrically shielded room, a 19" CRT monitor was used to deliver the stimuli, while in the MR scanner the stimuli were presented via a DLP projector (NEC N41, resolution of 1280x1024 @ 75 Hz refresh) onto a framed screen with translucent white tracing paper. A rear-projection technique projected the stimulus from the MR console window to the end of the MR bore and enabled stimuli to be clearly seen on screen via angled mirrors mounted onto the receiver head coil.

C. Pre-processing

The EEG was band pass filtered between 0.3 Hz and 40 Hz using a 4th order Butterworth filter (Matlab) and downsampled to 500 Hz. Differences in stimulus trigger delays resulting from the two types of presentation hardware were manually corrected. Heart beats (QRS complexes) were detected in the ECG using the FMRIB 1.21 plug-in. Detected beat times were shifted forward by 0.21s to align with the BCG peak and used for all three removal methods investigated [2].

D. Average artifact subtraction - AAS

The AAS method [2] as implemented in FMRIB 1.21 plug-in for EEGLAB [4] computes an artifact template for each occurring artifact by taking the mean of K artifacts around the current artifact (here $K = 20$). The template length is determined by the mean and the standard deviation of the heart beat intervals. This template is subtracted from the data epoch to remove the artifact. This moving average subtraction process is repeated for each channel.

E. Optimal basis set - OBS

The OBS method [3] defines the artifact template based on the first few principle components of a channel-wise temporal principle component analysis (PCA) of all artifacts present in a channel. These principal components or basis functions ideally describe the temporal variations of the artifacts and are fitted to each artifact and subtracted. The first three principle components were used. In this study the OBS implementation of the FMRIB 1.21 plug-in for EEGLAB [4] is used.

F. Matching Pursuit (MP) signal decomposition

MP is a signal decomposition method, which can be used to create signal approximations via a linear combination of so called time frequency-atoms g_{γ_n} out of a highly redundant dictionary [5, 6]. The different steps of the MP signal decomposition algorithm are briefly described as follows ([5]):

$$f = \sum_{n=0}^{m-1} \left\langle R^n f, g_{\gamma_n} \right\rangle \cdot g_{\gamma_n} + R^m f \qquad (1)$$

where f is the signal, $R^n f$ is the nth residuum, g_{γ_n} is the nth atom with parameters γ_n, $R^m f$ is the final residuum. Step 1: the algorithm systematically searches the dictionary for the atom g_{γ_n} with the highest correlation, i.e. the biggest inner product $\left\langle R^n f, g_{\gamma_n} \right\rangle$, with the residual signal $R^n f$. In the very first step the residual signal is identical with the signal to be decomposed. Step 2: Subtract the found atom from the residual signal. Continue back to step 1 with the new residual signal. Steps 1 and 2 are repeated until the desired number m of atoms is reached or the energy of the last computed residuum $R^m f$ is below a chosen level.

Different types of atoms can be used for MP decomposition. We use a dictionary built up by Gabor atoms, i.e. scaled, translated and modulated Gauss functions:

World Academy of Science, Engineering and Technology
International Journal of Biomedical and Biological Engineering
Vol:5, No:8, 2011

$$g_{(\gamma,\phi)}(t) = \frac{K_{(\gamma,\phi)}}{\sqrt{s}} \cdot g(\frac{t-u}{s}) \cdot \cos(ft+\phi), \text{ with } \gamma = (s,u,f) \quad (2)$$

where $g_{(\gamma,\phi)}$ is a Gabor atom, s is the scale, u is the translation, f is the modulation, ϕ is the phase, $K_{(\gamma,\phi)}$ is the amplitude, and $g(t)$ is a Gaussian function.

Gabor atoms have optimal time-frequency localization. With a highly redundant Gabor dictionary it is possible to create precise approximations of complicated signals with a relatively small number of parameterized atoms. This parameterization simplifies further signal processing.

G. Matching pursuit based removal

Our MP based removal method is schematized in Fig. 1. As mentioned in Section F, the EEG of the nth channel EEG_n is segmented into heartbeat related intervals $RR_{n,i}$ (RR-intervals) indexed by i. The MP approach models a cardiac pulse-related artifact template $Templ_{n,k}*$ by a matrix of weights C_{gab} multiplied by a Gabor dictionary Φ_{gab}. For this purpose, the heartbeat intervals' ($RR_{n,i}$) timing events are shifted firstly by 0.21s to align approximately with the respective maxima of each cardiac pulse-related artifact per $RR_{n,i}$ interval. Subsequently, the whole $RR_{n,i}$ sequence is subdivided into N non-overlapping blocks $B_{n,k}*$ of M=40 adjacent intervals and indexed by k. Then an artifact master template $Templ_{n,k}$ is computed for the modeling process by averaging the artifact occurrences of a given block of time-shifted RR-intervals. The template length is defined by the maximal RR-interval of the block. To avoid template overlap problems, the template was adaptively shortened to the current RR-interval in the later subtraction step. After the MP approximation of the artifact template to up to 50% of the residual energy, the template block model is iteratively adapted (constrained simplex downhill) to and subtracted from each artifact occurrence of all $RR_{n,i}*$ within a given block. The adaptation constraints for Gabor atoms were: scale: ± 15ms, translation: ± 25ms, modulation (i.e. frequency): ± 0.2Hz. The algorithm is repeated for all blocks per channel and for all channels. A final AAS-cleaning step removes the remaining deterministic artifact residuals. We therefore refer to this method as MP+AAS.

H. Validation Metrics

The **signal to noise ratio (SNR)** per channel was defined as:

$$SNR = \frac{|A_{P100}|}{std(noise)} \quad (3)$$

where

$$noise = \frac{2}{N} \cdot (\sum_{i=1}^{N/2} epoch_{2i-1} - \sum_{i=1}^{N/2} epoch_{2i}) \quad (4)$$

and where A_{P100} is the amplitude of the P100 component, *noise* refers to the residual noise in the averaged VEP, N is the number of VEP epochs, $epoch_{2i-1}$ is the ith odd VEP epoch, and $epoch_{2i}$ is the ith even VEP epoch [6]. To capture the SNR of the VEP selectively and robustly, the overall SNR was defined as the mean of the SNRs of the electrodes at the left
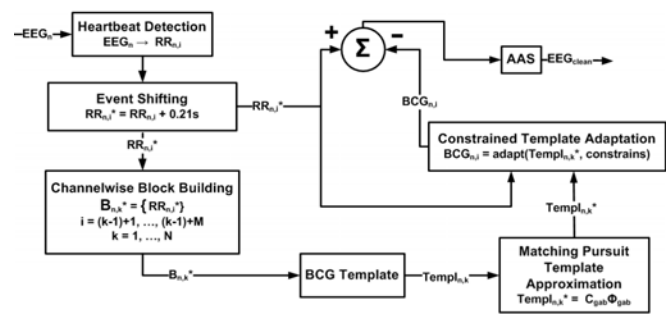

Fig. 1 Block diagram of matching pursuit based BCG removal.

occipital site of maximal VEP activation (channels 19, 21, 23, 41, 43, 45 and 47).

The **relative difference measure (RDM*)** of the P100 component was defined as:

$$RDM* = \sqrt{\sum_{i=1}^{M}\left(\frac{V_i^R}{\sqrt{\sum_{j=1}^{M}V_j^{R^2}}} - \frac{V_i^{BCG}}{\sqrt{\sum_{j=1}^{M}V_j^{BCG^2}}}\right)^2} \quad (5)$$

where M is the number of channels, V_i^R, V_j^R refer to the reference potentials (obtained outside the scanner) at the P100 VEP latency of the ith / jth channel, respectively; and V_i^{BCG}, V_j^{BCG} refer to the artifact affected potentials (obtained inside scanner) at the P100 VEP latency of the ith / jth channel, respectively. Note that the RDM* mainly specifies the differences of normalized spatial patterns [8].

The **relative magnitude error (rMAG)** of the P100 component was defined as:

$$rMAG = \sqrt{\frac{\sum_{i=1}^{M}V_i^{BCG^2}}{\sum_{i=1}^{M}V_i^{R^2}}} - 1 \quad (6)$$

where M is the number of channels, V_i^R is the reference potential (outside scanner) at VEP latency of the ith / jth channel; V_i^{BCG} is the affected potential (inside scanner) at VEP latency of the ith / jth channel [8].

I. Source Reconstruction

A person-specific boundary element model (skin (triangle side length 9 mm), outer skull (8 mm), inner skull (6 mm)) was constructed from a 1mm isotropic MPRAGE volume prior to cap application in Curry 7 (Compumedics Neuroscan, Hamburg, Germany). The electrode positions were manually derived from a subsequent MPRAGE volume acquired while the participant was wearing the electrode cap. Channels exceeding 60 kΩ were rejected; a common average reference was applied. A single cortically constrained dipole was fitted to the filtered and averaged P100 for each of the five conditions.
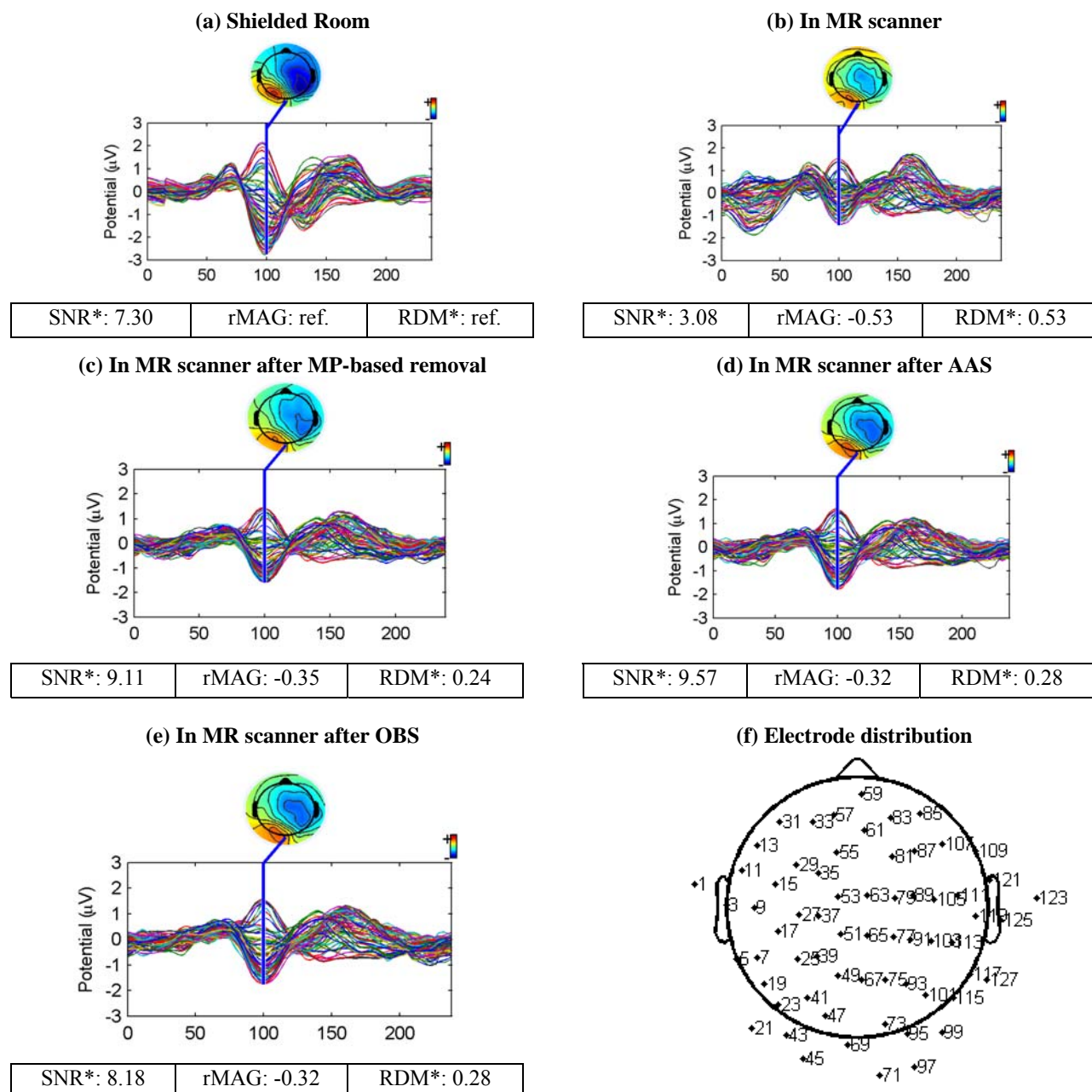
World Academy of Science, Engineering and Technology
International Journal of Biomedical and Biological Engineering
Vol:5, No:8, 2011

(a) Shielded Room

| SNR*: 7.30 | rMAG: ref. | RDM*: ref. |

(b) In MR scanner

| SNR*: 3.08 | rMAG: -0.53 | RDM*: 0.53 |

(c) In MR scanner after MP-based removal

| SNR*: 9.11 | rMAG: -0.35 | RDM*: 0.24 |

(d) In MR scanner after AAS

| SNR*: 9.57 | rMAG: -0.32 | RDM*: 0.28 |

(e) In MR scanner after OBS

| SNR*: 8.18 | rMAG: -0.32 | RDM*: 0.28 |

(f) Electrode distribution

Fig. 2 Channel plots (latency-corrected) and averaged P100 recorded in a shielded room (a), inside the static field of the MR scanner (b), after correction with the matching pursuit based method (c), after correction with AAS (d) and after correction with OBS (e). Subfigure (f) shows the electrode distribution. In (a)-(e) the contour increment is 0.5 µV.

III. RESULTS

A. Signal Magnitude

All removal methods show a decreased magnitude of P100 compared to the shielded room recording, resulting in negative rMAG values (Fig. 2). Regarding the BCG affected P100 magnitude in the MR scanner, the MP-based approach improved the relative magnitude error from rMAG=-0.53 to rMAG=-0.35. Both, AAS and OBS, arrive at a marginally lower error of rMAG=-0.32.

B. Field map Topography

The MP-based removal algorithm corrects the displacement of the negative maximum (right side of head) towards the center caused by the artifact (Fig. 2 (c), Fig. 3 top row). This is reflected in a lower topographic deviation value of RDM*=0.24 compared to the other removal methods. The displacement and broadening of the negative pole caused by the artifacts is only partially corrected by AAS and OBS, which results in higher topographic deviation value of RDM*=0.28 respectively.

World Academy of Science, Engineering and Technology
International Journal of Biomedical and Biological Engineering
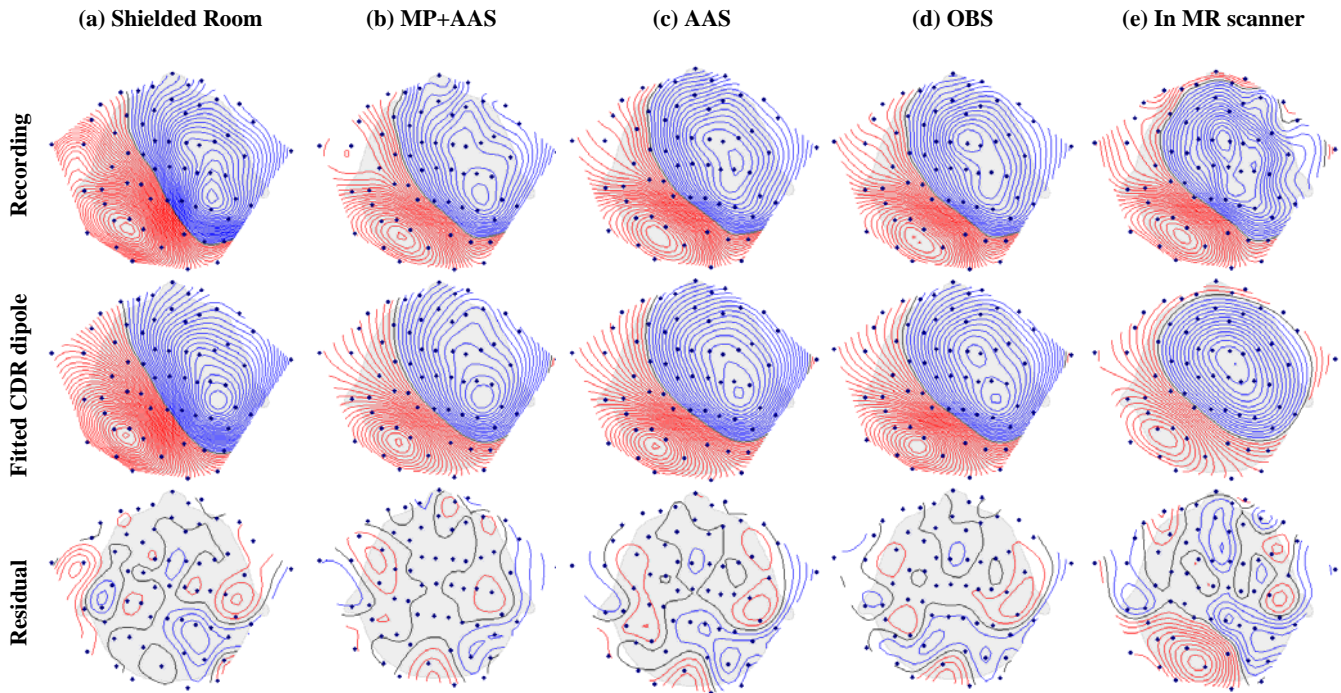Vol:5, No:8, 2011

Fig. 3 Field maps of averaged P100 in the shielded room (a), inside the static field of the MR scanner after correction with the matching pursuit based method (b), after correction with AAS (c), after correction with OBS (d) and inside the static field of the MR scanner (e).

C. Source Analysis

The source location of the VEP recorded inside the MR scanner is shifted by 14 mm posterior-superior from the source location of the artifact-free shielded room recording (Fig. 4, Table 1) in the right hemisphere. The OBS cleaned VEP source is even further away (18 mm) inferiorly from the artifact-free source. The MP and the AAS cleaned VEP source locations are very similar and about 8 mm from the artifact-free one. The explained variance is above 98% for all except the uncleaned recording where it is 91.7% (Table 1). This indicates that the removal algorithms were effective in removing artifact variance (shown as residual field maps in Fig. 3 bottom row). The source orientations of all five conditions are very similar, with the uncleaned MR-scanner VEP having the largest deviation.

D. Individual artifact occurrences

The removal of individual artifact occurrences is still frequently incomplete for AAS, OBS and MP+AAS respectively (Fig. 5). In this data set, the MP+AAS approach reduces the artifact amplitude and morphological components of the artifact to a larger degree than AAS and OBS.

TABLE I
PARAMETERS OF FITTED DIPOLE OF VEP (P100); X = LEFT TO RIGHT, Y = POSTERIOR TO ANTERIOR, Z = INFERIOR TO SUPERIOR.

	X [mm]	Y [mm]	Z [mm]	Explained Variance [%]	Distance [mm]
Sh. room	4.8	-46.0	60.3	99.45	ref.
MP+AAS	9.0	-52.7	56.6	98.75	8.7
AAS	5.0	-51.0	55.2	98.76	7.1
OBS	11.2	-56.5	47.2	99.34	18.0
Inside MR	-2.9	-57.6	59.3	91.68	14.0

IV. DISCUSSION

In this sample dataset, the matching pursuit based removal of cardiac pulse-related artifacts outperforms average artifact subtraction and optimal basis set method, in particular in topographical aspects which are of high significance for source reconstruction. While the presented MP-based artifact removal algorithms performed comparatively well in terms of
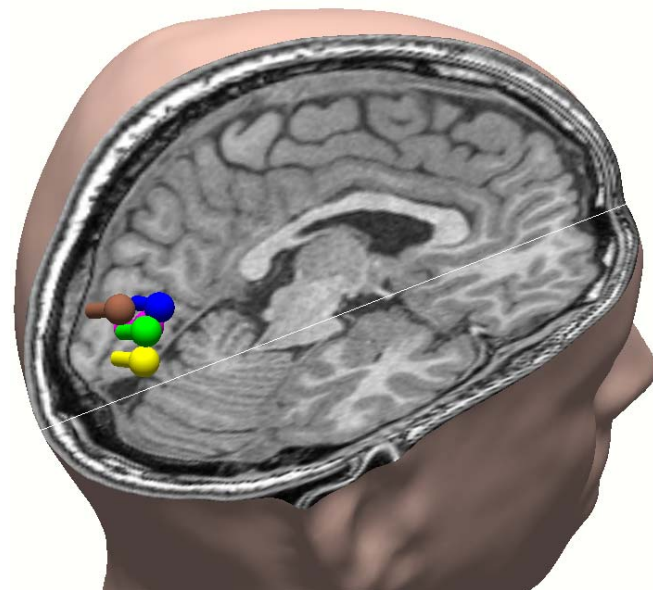

Fig. 4 Dipoles fitted to averaged P100 in the shielded room (brown, top left), inside the MR scanner (blue, top right), after OBS cleaning (yellow, bottom), MP+AAS cleaning (green, center) and AAS cleaning (magenta, coinciding with MP+AAS).

World Academy of Science, Engineering and Technology
International Journal of Biomedical and Biological Engineering
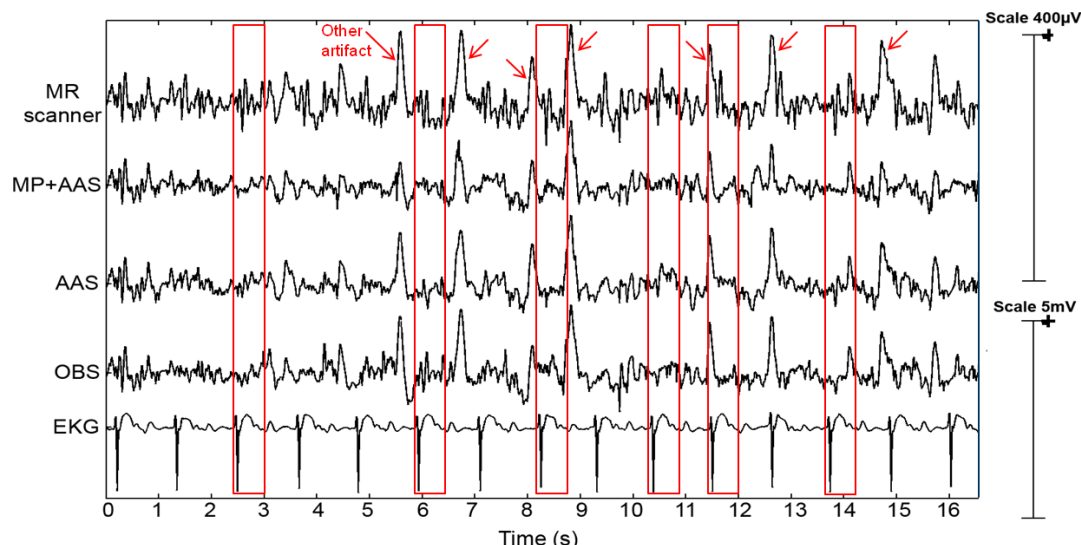Vol:5, No:8, 2011

Fig. 5 EEG sample (channel 59) recorded in the MR scanner with CPAs (top row), after application of MP+AAS (second row), after application of AAS (third row) and after application of OBS (fourth row). Selected CPAs highlighted with red rectangles show that MP+AAS removal is often more efficient than AAS or OBS removal, in particular for outlier artifacts, which differ in amplitude and/or morphology from neighboring artifacts. In the presence of other overlaid artifacts (indicated with red arrows) MP+AAS removes components of the other artifacts that are similar in morphology, frequency, phase and amplitude.

source localization, the interaction of the signal decomposition at the artifact removal stage and at the source reconstruction stage has to be considered. When fitting a single dipole model, the dominant dipolar moment will be separated from smaller, partially cardiac pulse-related and partially VEP-related signal components. It may therefore be the case that the source reconstruction seems accurate even though the artifact-removal is incomplete but of a beneficial nature. The favorable approach is of course to remove the artifact as early as possible in the signal processing queue and based on preferably unprocessed features to prevent compounded or enmeshed artifact removal problems in the high-level analysis.

The conceptual advantage of matching pursuit is that it can adapt to individual variations of artifact occurrences while still utilizing a common template. The degree of adaptation can be controlled separately for relevant features like latency, amplitude and frequency. AAS is restricted to artifact features that are persistent across a certain time interval, e.g. 10-20 occurrences. OBS is able to adapt the amplitude for each of the basis functions, but not latency or frequency variations.

In this case study, a trade-off in the parameterization of matching pursuit is the need to choose the adaptation constraints and thresholds and to interactively confirm the efficiency of the removal. From Fig. 5 is seems obvious that higher adaptation rates are required to achieve a more complete removal of the cardiac pulse-related artifacts. A larger dataset representing the full complexity of the cardiac pulse-related artifacts should be used to establish default parameters and to automate parameter adaptation to the individual recording.

V. CONCLUSION

Isolating the physiologically variable cardiac pulse-related artifacts in EEG recorded inside an MR scanner is a challenging problem, in particular for the analysis of single trial events, such as epileptic interictal and ictal discharges. The presented matching pursuit based approach showed promising results and new opportunities for parameterizing the removal process.

REFERENCES

[1] S. Debener, C. Kranczioch, and I. Gutberlet, "EEG Quality: Origin and Reduction of the EEG Cardiac-Related Artefact," in *EEG-fMRI: Physiological Basis, Technique and Applications*, C. Mulert and L. Lemieux, Ed. Berlin: Springer, 2010, p. 539.

[2] P. J. Allen, G. Polizzi, K. Krakow, D. R. Fish, et al., "Identification of EEG events in the MR scanner: the problem of pulse artifact and a method for its subtraction," *NeuroImage*, vol. 8, pp. 229-39, 1998.

[3] R. K. Niazy, C. F. Beckmann, G. D. Iannetti, J. M. Brady, and S. M. Smith, "Removal of FMRI environment artifacts from EEG data using optimal basis sets," *NeuroImage*, vol. 28, pp. 720-37, 2005.

[4] A. Delorme and S. Makeig, "EEGLAB: an open source toolbox for analysis of single-trial EEG dynamics including independent component analysis," *J Neurosci Methods*, vol. 134, pp. 9-21, 2004.

[5] M. Gratkowski, J. Haueisen, L. Arendt-Nielsen, A. C. Chen, and F. Zanow, "Decomposition of biomedical signals in spatial and time-frequency modes," *Methods Inf Med*, vol 47, pp. 26-37, 2008.

[6] M. Gratkowski, J. Haueisen, L. Arendt-Nielsen, A.C. Chen, and F. Zanow," Time-frequency filtering of MEG signals with matching pursuit". *J Physiol Paris*, vol. 99, pp. 47-57, 2006.

[7] H. Schimmel, "The (+) reference: accuracy of estimated mean components in average response studies," *Science*, vol. 157, pp. 92-4, 1967.

[8] J. W. Meijs, O. W. Weier, M. J. Peters, and A. van Oosterom, "On the numerical accuracy of the boundary element method," *IEEE Trans Biomed Eng*, vol 36, pp. 1038-49, 1989.